PHYSICAL REVIEW B **85**, 155422 (2012)

Near-field thermal radiation transfer controlled by plasmons in graphene

Ognjen Ilic,[1,*] Marinko Jablan,[2] John D. Joannopoulos,[1] Ivan Celanovic,[3] Hrvoje Buljan,[2] and Marin Soljačić[1]
[1]*Department of Physics, Massachusetts Institute of Technology, 77 Massachusetts Avenue, Cambridge, Massachusetts 02139, USA*
[2]*Department of Physics, University of Zagreb, Bijenička c. 32, 10000 Zagreb, Croatia*
[3]*Institute for Soldier Nanotechnologies, Massachusetts Institute of Technology, 77 Massachusetts Avenue, Cambridge, Massachusetts 02139, USA*

(Received 15 March 2012; published 11 April 2012)

It is shown that thermally excited plasmon-polariton modes can strongly mediate, enhance, and tune the near-field radiation transfer between two closely separated graphene sheets. The dependence of near-field heat exchange on doping and electron relaxation time is analyzed in the near infrared within the framework of fluctuational electrodynamics. The dominant contribution to heat transfer can be controlled to arise from either interband or intraband processes. We predict maximum transfer at low doping and for plasmons in two graphene sheets in resonance, with orders-of-magnitude enhancement (e.g., 10^2 to 10^3 for separations between 0.1 μm and 10 nm) over the Stefan-Boltzmann law, known as the far-field limit. Strong, tunable, near-field transfer offers the promise of an externally controllable thermal switch as well as a novel hybrid graphene-graphene thermoelectric/thermophotovoltaic energy conversion platform.

DOI: 10.1103/PhysRevB.85.155422 PACS number(s): 78.67.Wj, 73.20.Mf

I. INTRODUCTION

Heat transfer between two bodies can be greatly enhanced in the near field, i.e., by bringing their surfaces close together to allow tunneling of evanescent photon modes. For two parallel, semi-infinite, dielectric surfaces of index of refraction n, maximum flux enhancement is known to be n^2 times the Planck's blackbody limit.[1] However, particularly interesting near-field radiation transfer phenomena involve thermal excitation of various surface modes. Due to their localization and evanescent nature, it is only at submicron separations that these modes become relevant. Measuring near-field transfer has been experimentally difficult;[2–6] nevertheless, the promise of order-of-magnitude enhancement over the far-field Planck's blackbody limit has made near-field transfer the topic of much research.[7] A promising class of materials for enhancing the near-field transfer are plasmonic materials, due to the high density of modes around the frequency of plasmons. The potential of graphene[8] as a versatile and tunable plasmonic material has already been recognized in applications such as teraherz optoelectronics and transformation optics.[9–13] Unlike in metals, where high plasma frequencies make thermal excitation of surface modes difficult, plasmon frequencies in graphene can be anywhere from the teraherz to the near infrared.[14] In addition, the dependence of graphene conductivity on chemical potential, which in turn can be controlled by doping or by gating, allows for a tunable plasmonic dispersion relation. Transfer between graphene and amorphous SiO_2,[15,16] as well as application of graphene as a thermal emitter in a near-field thermophotovoltaic (TPV) system, has been reported.[17] Here we analyze the contribution of plasmon polaritons to graphene-graphene near-field heat transfer. The choice of identical coupled systems is predicated on the idea that resonant enhancement could lead to even greater heat transfer capacity. Indeed, we find maximal transfer for resonantly coupled plasmon modes (corresponding to similar doping in the two graphene sheets), which can be orders of magnitude larger than the heat transfer between two blackbodies in the far field.

In general, the radiative heat transfer between two bodies at temperatures T_1 and T_2 is given by

$$H = \int_0^\infty d\omega \left[\Theta(\omega, T_1) - \Theta(\omega, T_2)\right] f(\omega; T_1, T_2), \quad (1)$$

where $\Theta(\omega, T) = \hbar\omega/(e^{\hbar\omega/k_b T} - 1)$ is the average energy of a photon at frequency ω (the Boltzmann factor), and $f(\omega; T_1, T_2)$ is the spectral transfer function, characterizing frequency dependence of the heat exchange (i.e., how much heat is exchanged at a given frequency). In the context of fluctuational electrodynamics,[18] the spectral transfer function $f(\omega; T_1, T_2)$ is calculated in the following way: thermal fluctuations in the first (emitter) medium induce correlations between electric currents, which are proportional to the real part of the medium conductivity;[19] next, using Green functions, we can find the electromagnetic fields in the second (absorber) medium induced by the fluctuating currents in the first;[20] finally, the radiation transfer is obtained by calculating the Poynting flux around (or the ohmic losses within) the second medium. This approach has been used to numerically calculate the near-field transfer between two half-spaces,[18,21] as well as generalizations such as two slabs,[22] sphere and a plane,[3,23] and two spheres,[24] as well as one-dimensional (1D) periodic structures.[25]

II. PLASMONS AND NEAR-FIELD TRANSFER IN GRAPHENE

The system we analyze, shown in Fig. 1, consists of a suspended graphene sheet at temperature T_1 emitting to another suspended graphene sheet held at room temperature $T_2 = 300$ K, and a distance D away. In general, the p-polarization spectral transfer function for evanescent modes between two bodies is

$$f_p(\omega; T_1, T_2) = \frac{1}{\pi^2} \int_{\omega/c}^\infty dq\, q \frac{\mathrm{Im}\left(r_1^p\right) \mathrm{Im}\left(r_2^p\right)}{\left|1 - r_1^p r_2^p e^{2i\gamma D}\right|^2} e^{2i\gamma D}, \quad (2)$$

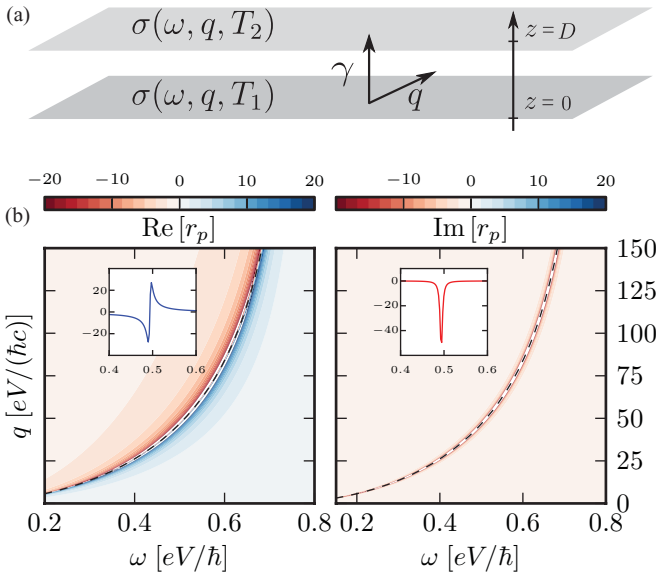

FIG. 1. (Color online) (a) Schematic diagram of the radiation transfer problem: a suspended sheet of graphene at temperature T_1 is radiating to another suspended graphene sheet at temperature T_2 and distance D away. k-vector components are q,γ, for the parallel and perpendicular component, respectively. (b) Real and imaginary parts of graphene p-polarization reflection coefficient for $\mu = 0.5$ eV, $T = 300$ K, and $\tau = 10^{-13}$ s. Dashed line is the vacuum plasmon dispersion relation (4) for the graphene sheet. Insets show the real and imaginary part of reflectivity at $q \approx 50$ eV/$\hbar c$ as a function of ω.

where $\gamma = \sqrt{\omega^2/c^2 - q^2}$ is the perpendicular wave vector and $r_{1(2)}$ is the reflection coefficient for the bottom (top) body; note that $r_{1,2}$ depend on T, and hence the T dependence of $f(\omega, T_1, T_2)$. Integration is over the parallel wave vector q, limited only to the evanescent ($q > \omega/c$) modes. The spectral transfer function (2) was derived for the case of two semi-infinite slabs;[7] however, it can be shown that the same expression is valid when any of the two bodies is a 2D system, such as graphene.[17] Since graphene absorbs poorly (2.3%) in the far field (hence is also a poor emitter), not including the propagating modes is a good approximation. The contribution of evanescent s-polarized modes can also be calculated using Eq. (2), but it turns out to be negligible compared to p-polarized modes, as we discuss later. We assume graphene is completely characterized by its complex optical conductivity $\sigma = \sigma_r + i\sigma_i$, which depends on angular frequency ω, electron scattering lifetime τ, chemical potential μ, and temperature T. Furthermore, the graphene conductivity is taken to be independent of the parallel wave vector q (see discussion below), and consists of the Drude (intraband) and interband conductivity, expressed respectively as[26]

$$\sigma_D = \frac{i}{\omega + i/\tau}\frac{e^2 2k_b T}{\pi\hbar^2}\ln\left[2\cosh\frac{\mu}{2k_b T}\right],$$
$$\sigma_I = \frac{e^2}{4\hbar}\left[G\left(\frac{\hbar\omega}{2}\right) + i\frac{4\hbar\omega}{\pi}\int_0^\infty \frac{G(\xi) - G(\hbar\omega/2)}{(\hbar\omega)^2 - 4\xi^2}d\xi\right], \quad (3)$$

where $G(\xi) = \sinh(\xi/k_b T)/[\cosh(\mu/k_b T) + \cosh(\xi/k_b T)]$ and μ is the chemical potential. Various electron scattering processes are taken into account through the relaxation time τ. From dc mobility measurements in graphene, one obtains[9] an order-of-magnitude value of $\tau \approx 10^{-13}$ s.

First we discuss the electrodynamic properties of a single suspended sheet of graphene, inherent in the p-polarization reflection coefficient, which is illustrated in Fig. 1(b). The reflection coefficient is $r_p = (1 - \epsilon)/\epsilon$, where $\epsilon = 1 + \gamma\sigma/(2\epsilon_0\omega)$ is the dielectric function of graphene.[26] Its pole $\epsilon = 0$ corresponds to the dispersion relation of p-polarized plasmon modes[9]

$$q = \epsilon_0 \frac{2i\omega}{\sigma(\omega, T)}, \quad (4)$$

which is shown as the dashed line in Fig. 1(b). Figure 1 shows plasmons exist in a strongly nonretarded regime ($q \gg \omega/c$), indicating a tightly confined plasmon polariton mode. Graphene also supports s-polarized surface modes with a dispersion relation very close to the light line.[27] However, due to the large density of states and the tightly confined nature of p-polarized surface modes, it is the p polarization that dominates (as our calculations confirm) the near-field transfer.

III. RESULTS AND ANALYSIS

When two parallel graphene sheets are sufficiently close [see Fig. 1(a)], their plasmonic modes can become coupled. The dispersion of these coupled modes is $1 - r_1^p(\omega) r_2^p(\omega) e^{-2qD} = 0$, when $q \gg \omega/c$, so $\gamma \approx iq$, which is exactly the pole of the integrand of the spectral transfer function (2). The integrand is illustrated in Fig. 2 for different values of chemical potential. The coupling of modes is strongest

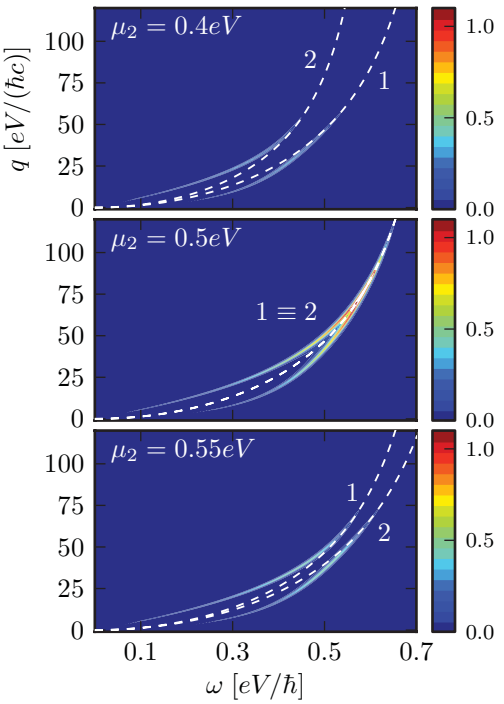

FIG. 2. (Color online) Contour plot of the integrand (a.u.) in $f_p(\omega)$ from Eq. (2), for two graphene sheets at $T_{1,2} = 300$ K, separated by $D = 10$ nm. Chemical potentials are $\mu_1 = 0.5$ eV, while μ_2 is different for each plot. Dashed lines correspond to the vacuum plasmon dispersion relations for the bottom (1) and the top (2) graphene sheet.

when both graphene sheets have identical parameters (middle panel in Fig. 2). In that case, their individual dispersions are identical. Nevertheless, the dispersion of the combined system shows two branches that dominate the near-field spectral transfer, i.e., the implicit equation $1 - r(\omega)^2 e^{-2qD} = 0$ for $\omega(q)$ has two explicit solutions: $\omega_{\text{even}}(q)$ and $\omega_{\text{odd}}(q)$ for the even and the odd mode, respectively. The splitting of two superimposed resonances is particularly noticeable at smaller wave vectors q. For larger q, the splitting disappears, and the resonant matching of peaks of $\text{Im}(r_{1,2})$ significantly enhances the near-field transfer. As the chemical potential of one of the sheets changes (top and bottom panel in Fig. 2), the plasmons in the two sheets move out of resonance, coupling decreases, the peaks in the integrand approach the individual (vacuum) plasmons dispersion curves, and the heat transfer becomes lower than in resonance.

Figure 3(a) shows a highly tunable spectral transfer function f_p for different values of chemical potential and relaxation time. Given the chemical potential, the relaxation time determines which processes (interband or intraband) are responsible for the peaks in spectral transfer. Since interband processes are dominant at high frequencies, all τ curves converge in the high frequency limit, where Drude losses are negligible. However, interband processes can play a leading role even below the absorption threshold $\omega \approx 2\mu$, particularly for small chemical potential where thermal broadening of the interband threshold (on the order of few $k_b T$) becomes more significant. For example, for $\mu_{1,2} = 0.1$ eV [first peak in Fig. 3(a)] the similarity between $\tau = 10^{-12}$ s and $\tau = 10^{-13}$ s spectral transfer functions indicates that the majority of loss in

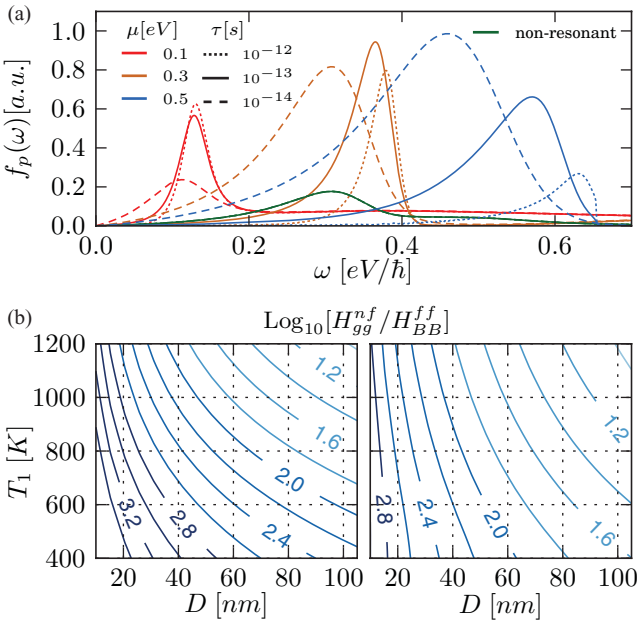

FIG. 3. (Color online) (a) Spectral transfer function $f_p(\omega)$ from Eq. (2), for plasmons in two graphene sheets at resonance, $\mu_{1,2} = \mu$, $\tau_{1,2} = \tau$; $T_{1,2} = 300$ K, $D = 10$ nm. Solid green line corresponds to the $\mu_{1(2)} = 0.3(0.5)$ eV, $\tau_{1(2)} = 10^{-13}(10^{-14})$ s case. (b) Contour plot of the integrated ratio of the near-field transfer between two graphene sheets, H_{gg}^{nf}, and the far-field transfer between two blackbodies, H_{BB}^{ff} for plasmons in resonance (left, $\mu_{1,2} = 0.1$ eV) and out of resonance [right, $\mu_{1(2)} = 0.1(0.3)$ eV]. Here, $T_2 = 300$ K and $\tau_{1,2} = 10^{-13}$ s.

graphene comes from interband processes. On the other hand, the Drude (intraband) loss term, usually important for $\omega < \mu$, can become dominant at higher frequencies, for large enough μ (third peak). Finally, a combination of two loss processes, $\mu_{1(2)} = 0.3(0.5)$ eV and $\tau_{1(2)} = 10^{-13}(10^{-14})$ s, can lead to a hybrid spectral transfer. While the use of q-independent expression for graphene conductivity Eq. (3) for intraband processes is a good approximation,[9] one must take care when applying Eq. (3) to interband transitions. As indicated in Fig. 3(a), interband transitions can play a significant role in near-field transfer at low doping levels. Here, the contribution from the nonzero wave vector becomes important since it broadens the interband threshold from 2μ to $\sim 2\mu - \hbar q v_F$. On the other hand, this is similar to nonzero temperature effects which also broaden the interband threshold, so we do not expect a qualitatively different result with q-dependent conductivity.

We quantify the heat exchange in the near-field by plotting [Fig. 3(b)] the integrated transfer H from Eq. (1) normalized to the transfer between two blackbodies in the far field. Factoring in the temperature dependence shifts the majority of the near-field transfer to lower frequencies, due to the exponentially decaying Boltzmann factor. This implies that, while doping or gating might be advantageous in some applications (for example, emitter-PV cell band-gap frequency matching in near-field TPV systems[17]), near-field transfer between two graphene sheets is maximized for small values of doping, despite the stronger peak in spectral transfer for $\mu_{1,2} = 0.3$ eV vs $\mu_{1,2} = 0.1$ eV [Fig. 3(a)]. For plasmons in resonance with $\mu_{1,2} = 0.1$ eV [left panel, Fig. 3(b)], we observe orders-of-magnitude increase in heat exchange, particularly at small separations ($\times 1000$ for $D = 20$ nm, $T_1 = 800$ K), but also at separations as large as 0.1 μm. At larger separations, we observe (not shown) the shift of the peak of the spectral transfer function f_p to $\mu_{1,2} = 0.1$ eV case [red line in Fig. 3(a)], indicating that the coupling between highly localized, large q, modes becomes weaker, and the transfer is dominated by lower-frequency, less evanescent modes. The heat transfer depends in a complex fashion on the parameters of the system, and does not seem to yield a simple functional dependence on the emitter and absorber temperatures (as is the case for two blackbodies). Nevertheless, there is a relative advantage [Fig. 3(b)] to operating at lower temperatures, as the temperature dependence of the near-field transfer appears to grow slower than the T^4 blackbody dependence. Finally, we note that the temperature dependence of conductivity reduces the resonant effect when two graphene sheets are at different temperatures. This reduction is more pronounced for a large temperature difference, shifting the peak of the spectral transfer on the order of $k_b T$; however, the relative reduction of the integrated spectral transfer function is small, with the main temperature dependence coming from the Boltzmann factor. This efficient heat exchange between two graphene sheets in the near field, together with recently reported advances in hot carrier extraction from graphene,[28] may offer a potential for a novel, hybrid thermophotovoltaic/thermoelectric solid-state heat-to-electricity conversion platform. In addition, this material system could pave the way toward an externally controllable thermal switch behavior, where one can, by means of doping or gating, tune the resonant coupling between the hot and the cold side.

Note added. Recently, we became aware of a related paper by Svetovoy, van Zwol, and Chevrier, where the contribution of plasmons to the near-field radiation transfer in graphene has also been analyzed.[29]

ACKNOWLEDGMENTS

The authors would like to acknowledge helpful discussions with Pablo Jarillo-Herrero, Nathan Gabor, Gang Chen, Alejandro Rodriguez, and Steven Johnson. O.I. and M.S. were partially supported by the MIT S3TEC Energy Research Frontier Center of the Department of Energy under Grant No. DE-SC0001299. M.J. was supported in part by the Croatian Ministry of Science under Grant No. 119-0000000-1015. This work was also partially supported by the Army Research Office through the Institute for Soldier Nanotechnologies under Contract No. W911NF-07-D0004, and the Unity through Knowledge Fund Grant Agreement No. 93/11.

*ilico@mit.edu

[1] L. D. Landau and E. M. Lifshitz, *Statistical Physics, Part 2* (Pergamon Press, New York, 1980).
[2] C. Hargreaves, Phys. Lett. A **30**, 491 (1969).
[3] A. Narayanaswamy, S. Shen, and G. Chen, Phys. Rev. B **78**, 115303 (2008).
[4] S. Shen, A. Narayanaswamy, and G. Chen, Nano Lett. **9**, 2909 (2009).
[5] E. Rousseau, A. Siria, G. Jourdan, S. Volz, F. Comin, J. Chevrier, and J.-J. Greffet, Nat. Photon. **3**, 514 (2009).
[6] R. S. Ottens, V. Quetschke, S. Wise, A. A. Alemi, R. Lundock, G. Mueller, D. H. Reitze, D. B. Tanner, and B. F. Whiting, Phys. Rev. Lett. **107**, 014301 (2011).
[7] K. Joulain, J.-P. Mulet, F. Marquier, R. Carminati, and J.-J. Greffet, Surf. Sci. Rep. **57**, 59 (2005).
[8] K. S. Novoselov, A. K. Geim, S. V. Morozov, D. Jiang, Y. Zhang, S. V. Dubonos, I. V. Grigorieva, and A. A. Firsov, Science **306**, 666 (2004).
[9] M. Jablan, H. Buljan, and M. Soljačić, Phys. Rev. B **80**, 245435 (2009).
[10] B. Wunsch, T. Stauber, F. Sols, and F. Guinea, New J. Phys. **8**, 318 (2006).
[11] E. H. Hwang and S. Das Sarma, Phys. Rev. B **75**, 205418 (2007).
[12] L. Ju, B. Geng, J. Horng, C. Girit, M. Martin, Z. Hao, H. A. Bechtel, X. Liang, A. Zettl, Y. R. Shen, and F. Wang, Nat. Nano **6**, 630 (2011).
[13] A. Vakil and N. Engheta, Science **332**, 1291 (2011).
[14] F. Rana, Nat. Nano **6**, 611 (2011).
[15] B. N. J. Persson and H. Ueba, J. Phys.: Condens. Matter **22**, 462201 (2010).
[16] A. I. Volokitin and B. N. J. Persson, Phys. Rev. B **83**, 241407 (2011).
[17] O. Ilic, M. Jablan, J. D. Joannopoulos, I. Celanovic, and M. Soljačić, Opt. Express **20**, A366 (2012).
[18] S. Rytov, Y. A. Kratsov, and V. I. Tatarskii, *Principles of Statistical Radiophysics* (Springer-Verlag, Berlin, 1987).
[19] H. A. Haus, J. Appl. Phys. **32**, 493 (1961).
[20] J. E. Sipe, J. Opt. Soc. Am. B **4**, 481 (1987).
[21] J. Pendry, J. Phys.: Condens. Matter **11**, 6621 (1999).
[22] P. Ben-Abdallah, K. Joulain, J. Drevillon, and G. Domingues, J. Appl. Phys. **106**, 044306 (2009).
[23] J.-P. Mulet, K. Joulain, R. Carminati, and J.-J. Greffet, Microscale Thermophys. Eng. **6**, 209 (2002).
[24] A. Narayanaswamy and G. Chen, Phys. Rev. B **77**, 075125 (2008).
[25] A. W. Rodriguez, O. Ilic, P. Bermel, I. Celanovic, J. D. Joannopoulos, M. Soljačić, and S. G. Johnson, Phys. Rev. Lett. **107**, 114302 (2011).
[26] L. A. Falkovsky, J. Phys. Conf. Ser. **129**, 012004 (2008).
[27] S. A. Mikhailov and K. Ziegler, Phys. Rev. Lett. **99**, 016803 (2007).
[28] N. M. Gabor, J. C. W. Song, Q. Ma, N. L. Nair, T. Taychatanapat, K. Watanabe, T. Taniguchi, L. S. Levitov, and P. Jarillo-Herrero, Science **334**, 648 (2011).
[29] V. B. Svetovoy, P. J. van Zwol, and J. Chevrier, eprint arXiv:1201.1824 (to be published in Phys. Rev. B).